# Lawrence Berkeley National Laboratory
## LBL Publications

## Title
Metaproteomics-informed stoichiometric modeling reveals the responses of wetland microbial communities to oxygen and sulfate exposure.

## Permalink

## Journal

## Authors
Wang, Dongyu
Candry, Pieter
Hunt, Kristopher
et al.

## Publication Date

## DOI

**Article**

# Metaproteomics-informed stoichiometric modeling reveals the responses of wetland microbial communities to oxygen and sulfate exposure

Check for updates

Dongyu Wang[1], Pieter Candry [2,3], Kristopher A. Hunt [2], Zachary Flinkstrom [2], Zheng Shi[1,4], Yunlong Liu[5], Neil Q. Wofford[1], Michael J. McInerney[1], Ralph S. Tanner[1], Kara B. De León [1], Jizhong Zhou[1,4,6,7], Mari-Karoliina H. Winkler [2], David A. Stahl[2] & Chongle Pan [1,5] ✉

Climate changes significantly impact greenhouse gas emissions from wetland soil. Specifically, wetland soil may be exposed to oxygen ($O_2$) during droughts, or to sulfate ($SO_4^{2-}$) as a result of sea level rise. How these stressors – separately and together – impact microbial food webs driving carbon cycling in the wetlands is still not understood. To investigate this, we integrated geochemical analysis, proteogenomics, and stoichiometric modeling to characterize the impact of elevated $SO_4^{2-}$ and $O_2$ levels on microbial methane ($CH_4$) and carbon dioxide ($CO_2$) emissions. The results uncovered the adaptive responses of this community to changes in $SO_4^{2-}$ and $O_2$ availability and identified altered microbial guilds and metabolic processes driving $CH_4$ and $CO_2$ emissions. Elevated $SO_4^{2-}$ reduced $CH_4$ emissions, with hydrogenotrophic methanogenesis more suppressed than acetoclastic. Elevated $O_2$ shifted the greenhouse gas emissions from $CH_4$ to $CO_2$. The metabolic effects of combined $SO_4^{2-}$ and $O_2$ exposures on $CH_4$ and $CO_2$ emissions were similar to those of $O_2$ exposure alone. The reduction in $CH_4$ emission by increased $SO_4^{2-}$ and $O_2$ was much greater than the concomitant increase in $CO_2$ emission. Thus, greater $SO_4^{2-}$ and $O_2$ exposure in wetlands is expected to reduce the aggregate warming effect of $CH_4$ and $CO_2$. Metaproteomics and stoichiometric modeling revealed a unique subnetwork involving carbon metabolism that converts lactate and $SO_4^{2-}$ to produce acetate, $H_2S$, and $CO_2$ when $SO_4^{2-}$ is elevated under oxic conditions. This study provides greater quantitative resolution of key metabolic processes necessary for the prediction of $CH_4$ and $CO_2$ emissions from wetlands under future climate scenarios.

Wetlands store approximately one-third of global soil organic carbon (SOC) and play important roles in regulating and stabilizing global climate[1–3]. $CH_4$ and $CO_2$, the two greatest contributors to the greenhouse effect, are the dominant gaseous end-products from the mineralization of organic carbon in wetland ecosystems[4,5]. Carbon fluxes in a wetland ecosystem are closely linked to its hydrological features[6]. Climate changes may introduce specific hydrology-related stressors. For instance, freshwater wetlands are

increasingly vulnerable to drought events, which lower water tables and introduce $O_2$ into wetland soils. This leads to more frequent exposure of soil organic matter to $O_2$, thereby affecting the organic carbon balance[7]. In addition, freshwater wetlands face perturbations as a result of seawater intrusions. As the sea level rises, the inundation of wetlands by seawater brings a high concentration of sulfate ions ($SO_4^{2-}$), substantially altering the sediment chemistry[2,8,9]. These stressors can change the production patterns of

[1]School of Biological Sciences, University of Oklahoma, Norman, OK, USA. [2]Department of Civil and Environmental Engineering, University of Washington, Seattle, WA, USA. [3]Laboratory of Systems and Synthetic Biology, Wageningen University & Research, Wageningen, The Netherlands. [4]Institute for Environmental Genomics, University of Oklahoma, Norman, OK, USA. [5]School of Computer Science, University of Oklahoma, Norman, OK, USA. [6]School of Civil Engineering and Environmental Sciences, University of Oklahoma, Norman, OK, USA. [7]Earth and Environmental Sciences, Lawrence Berkeley National Laboratory, Berkeley, CA, USA. ✉e-mail: cpan@ou.edu

**Fig. 1 | Schematic diagram of study design.**
Emissions of methane and carbon dioxide from wetland ecosystems can be severely perturbed by climate-change-induced stressors, such as seawater intrusions and droughts. To investigate this, we constructed laboratory microcosms using fresh-water wetland soils under four incubation conditions, including anoxic non-sulfate addition (S-O-), anoxic sulfate-addition (S+O-), oxic non-sulfate addition (S-O+) and oxic sulfate-addition (S+O+) conditions. The soil communities were characterized by integrating geochemical analysis, metagenomics, metaproteomics and stoichiometric modeling. The results uncovered the molecular mechanism on how wetland microbial communities modulate greenhouse gas fluxes under future climate scenarios.
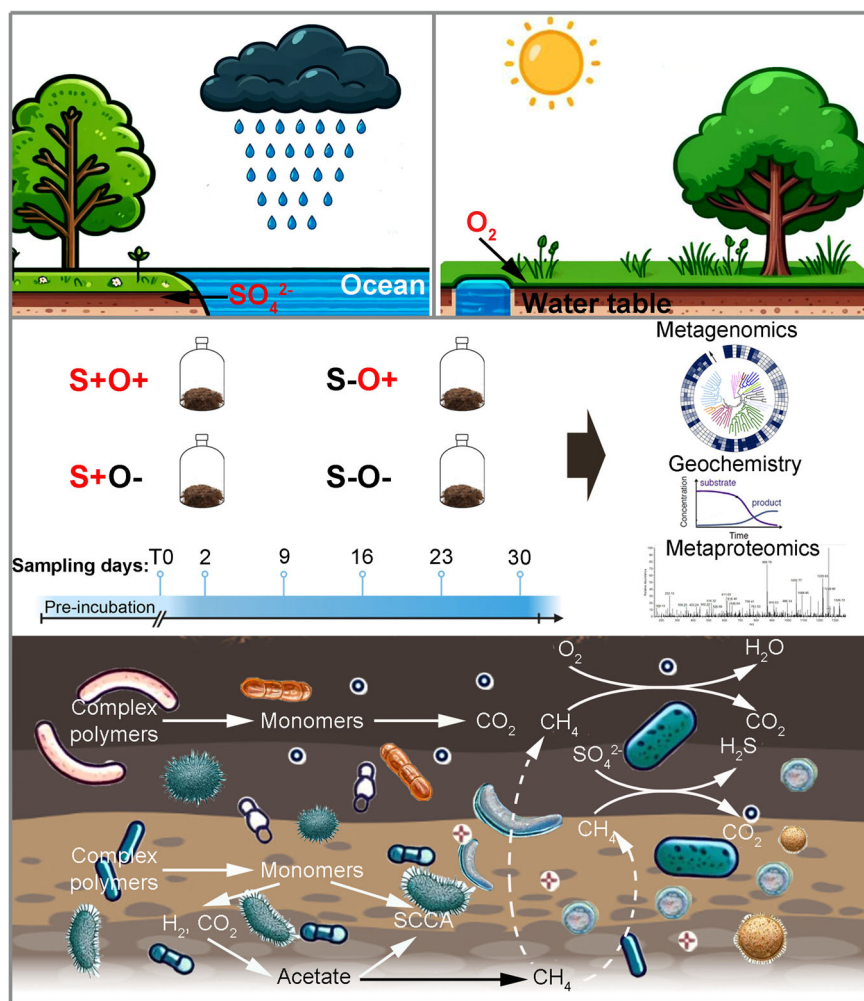


CH$_4$ and CO$_2$, resulting in feedback that is poorly characterized qualitatively in terms of the direction of the changes and quantitatively in terms of the magnitudes of the changes. Understanding how environmental disturbances affect the dynamic of metabolic processes and the succession of ecological communities is critical for accurately modeling changes in greenhouse gas emissions from wetland ecosystems in future climate scenarios.

Microbial interactions are vital in modulating organic matter decomposition and greenhouse gas emissions within wetland ecosystems[10,11]. These interactions are driven by fermentation and respiration, coupling the oxidation of organic compounds by electron transfer to electron acceptors[12–14]. In the absence of disturbance by droughts and seawater intrusions, obligatory anaerobic fermenters become dominant[15]. Syntrophic interactions among these diverse anaerobic microorganisms facilitate the stepwise breakdown of complex organic substrates into simpler, chemically stable compounds, ultimately resulting in the production of CH$_4$ and CO$_2$[16]. However, O$_2$ exposure introduced during drought can promote aerobic microbial respiration of carbon stocks, with CO$_2$ as the primary product[17]. The introduction of SO$_4^{2-}$ from seawater inundation as an alternative electronic acceptor leads to sulfate-reducing bacteria (SRB) to producing more H$_2$S, utilizing H$_2$ and/ or organic acids as electron donors. The competition from SRBs for H$_2$ and organic acids may reduce methane production by methanogens[18,19]. Characterizing these metabolic interactions provides insight into biochemical transformations within the community under changing redox conditions, and allows for investigations into how changes in these conditions, induced by climate change, will affect the microbial metabolic networks that control carbon cycling in wetland ecosystems.

Carbon cycling and gas emissions in wetlands have been studied extensively in both field and laboratory conditions[20–23]. Elevated CO$_2$ levels, reduced carbon accumulation, and decreased CH$_4$ emissions have been observed when introducing O$_2$ into previously anoxic wetland soil[22,24]. Previous studies have also demonstrated lower CH$_4$ emissions to the atmosphere from lacustrine wetlands following seawater intrusion [21-23]. However, few studies have characterized how the critical syntrophic interactions controlling CH$_4$ and CO$_2$ productions respond to environmental redox perturbations, such as increased O$_2$ from periods of drought or SO$_4^{2-}$ from seawater intrusion.

Establishing a clear connection between environmental disturbance and microbial adaptations remains a challenge, due to the complex and dynamic nature of microbial communities[25,26]. In this study, we set up laboratory microcosms to investigate the effects of SO$_4^{2-}$ exposure and O$_2$ exposure alone or in combination on microbial activities and interactions, as well as the resulting fate of carbon within wetland soil (Fig. 1). We used proteogenomics to characterize the biochemical and physiological responses of microbial communities to individual perturbations and their combined effects. Stoichiometric models were employed to deconvolute carbon exchanges among the main functional guilds. By integrating geochemical, metaproteomic, and stoichiometric analyses, we aimed to develop a molecular understanding of how climate change-induced stressors modulate wetland microbial communities and greenhouse gas fluxes.
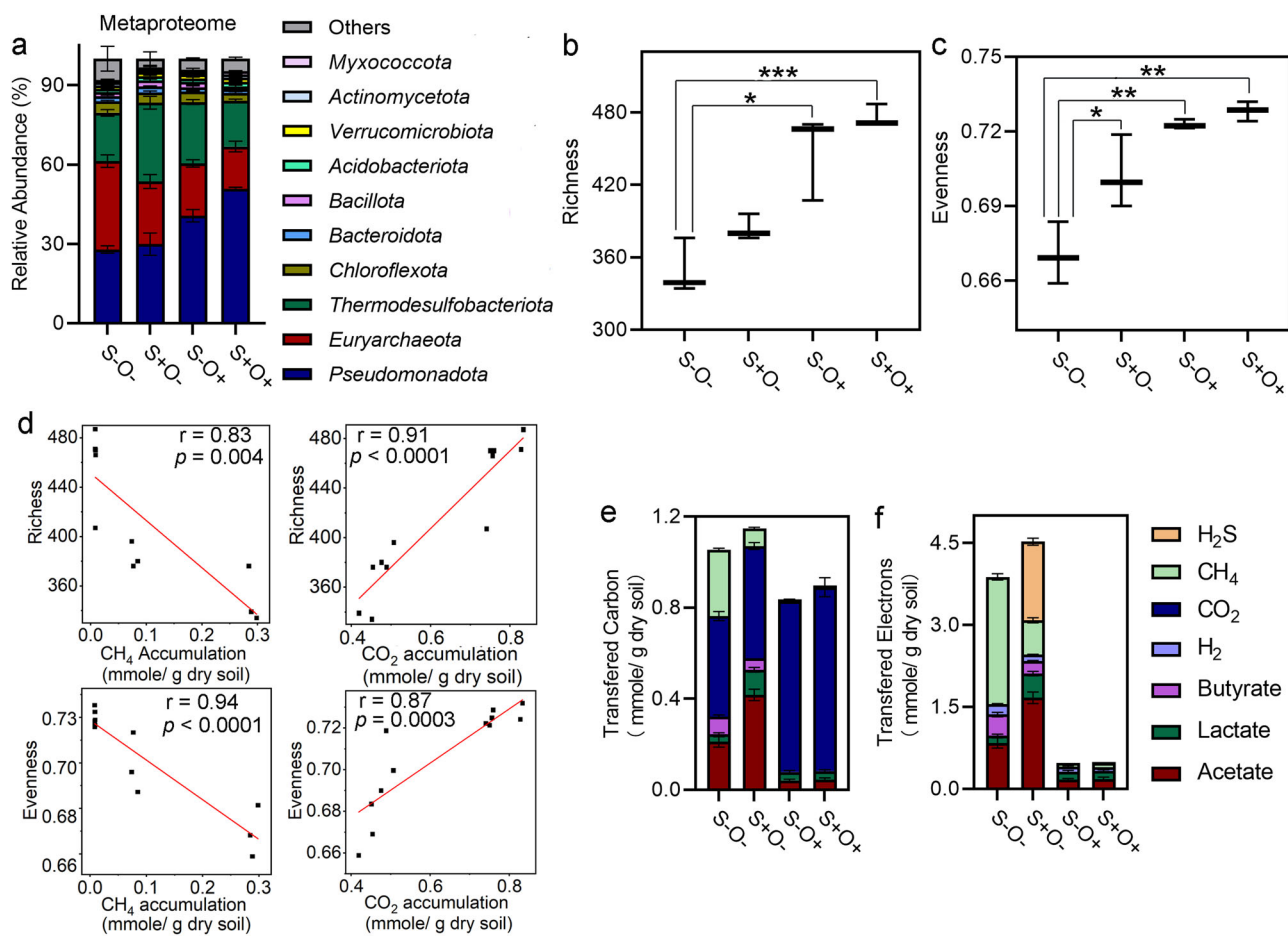
**Fig. 2 | Effects of $SO_4^{2-}$ and $O_2$ exposures on microbial community composition and activities. a** Relative proteomic abundance of microbial phyla under four treatment scenarios. The relative proteomic abundance is expressed as the proportion of total proteins attributable to each microbial species. **b, c** Community species diversity indices, with **b** showing the richness and **c** the evenness across the four experimental conditions. Significant differences with *p*-values determined using Student's t-test and adjusted for the false discovery rate, are marked by * for *p*-value < 0.05, ** for *p*-value < 0.01 and *** for *p*-value < 0.001. **d** Correlation between microbial species diversity and the accumulations of $CH_4$ and $CO_2$, where each dot represents an experimental measurement (X-axis for geochemical measurements, Y-axis for metaproteomic measurements) from the four conditions with three replicates, and the red line displays best linear fit. r is the Pearson correlation coefficient, and p values were determined by t-statistic. **e, f** Cumulative amounts of fermentation products are measured by carbon molarity **e** and electron molarity **f** within the microcosms. The error bars are defined as standard deviation.

## Results

### $SO_4^{2-}$ and $O_2$ additions changed community structure and activities

Laboratory microcosms were constructed using lacustrine wetland soils and incubated under four conditions: anoxic non-sulfate-addition (S-O-), anoxic sulfate-addition (S+O-), oxic non-sulfate-addition (S-O+), and oxic sulfate-addition (S+O+) (Fig. 1). Sterile air was introduced under S-O+ and S+O+ conditions. The final concentration of $SO_4^{2-}$ following addition under the S+O- and S+O+ conditions was approximately 7.2 mM, falling within the range of natural seawater concentration[27].

Metaproteomic analysis identified a total of 10598 proteins based on assignments of unique peptide identifications to individual proteins. These proteins originated from 807 microbial species and 50 phyla, with *Pseudomonadota* (~51% of total proteome abundance) and *Euryarchaeota* (~33% of total proteome abundance) being the dominant phyla (Fig. 2a and Supplementary Table 2). All experimental treatments resulted in an increase of *Pseudomonadota* in proteome abundance compared to the S-O- condition. However, the increase under dual exposure (S+O+, 82%, *p*-value < 0.000, t-test) was more than the additive effect of the increase observed under the S+O- condition (45%, *p*-value = 0.001, t-test) and S-O+ condition (7%, *p*-value = 0.5, t-test). This suggests a synergistic interaction between the effects of $SO_4^{2-}$ and $O_2$ on the proteome abundance of *Pseudomonadota*, where their combined impact on microbial communities is greater than the sum of their individual effects. Conversely, *Euryarchaeota* consistently decreased in proteome abundance upon stress exposure, although this reduction was less under dual exposure (S+O+, 52%, *p*-value = 0.0006, t-test) than the sum of the decreases under S+O- condition (29%, *p*-value = 0.008, t-test) and S-O+ condition (41%, *p*-value = 0.001, t-test) (Fig. 2a). This suggests an antagonistic interaction between the effects of $SO_4^{2-}$ and $O_2$ on the proteome abundance of *Euryarchaeota*, where their combined impact on microbial communities is less than the sum of their individual effects.

Compared to the S-O- condition, the metaproteome abundances of active communities showed increased richness under both the S+O- (28%, *p*-value = 0.02, t-test) and S-O+ conditions (36%, *p*-value = 0.0009, t-test). There was also an increase in evenness under S+O- (5%, *p*-value = 0.04, t-test) condition, S-O+ condition (8%, *p*-value < 0.002, t-test), and S+O+ condition (9%, *p*-value = 0.001, t-test) (Fig. 2b, c). This suggests that $SO_4^{2-}$ and $O_2$ exposures contributed to the proliferation of low-abundance microbial species. Moreover, we found a negative correlation between the increased richness and evenness of the active community and the accumulation of $CH_4$ and a positive correlation with $CO_2$ accumulation (Fig. 2d).

The primary metabolic products in the microcosm system were quantified by carbon (Fig. 2e) and electron molarity (Fig. 2f). Under the
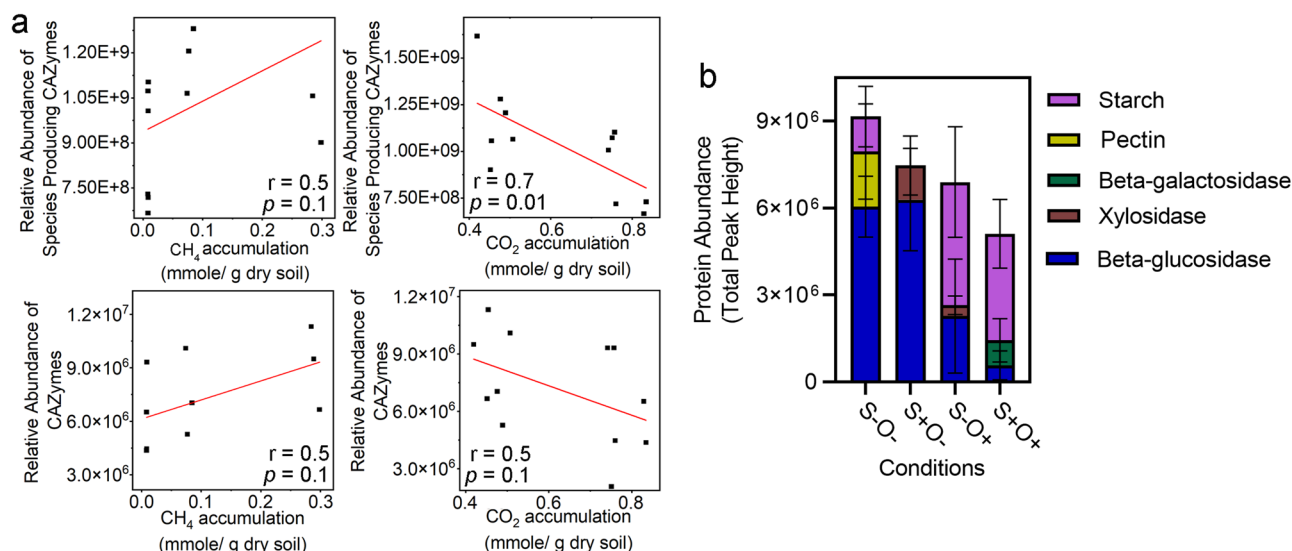
**Fig. 3 | Effects of $SO_4^{2-}$ and $O_2$ exposures on plant polysaccharide degradation.**
**a** Correlation analysis between the relative abundances of plant polymer degradation species and CAZymes with the accumulation of $CH_4$ and $CO_2$, where each dot represents experimental measurements (X-axis for geochemical measurements,

Y-axis for metaproteomic measurements) from four conditions with three replicates, and the red line is the result of linear fitting. r is the Pearson correlation coefficient, and $p$ values were determined by t-test. **b** Protein abundances of CAZyme under the four conditions. The error bars are defined as standard deviation.

S-O- condition, the soil carbon was fermented into $0.32 \pm 0.03$ mmole/g dry soil of organic acids, $0.44 \pm 0.02$ mmole/g dry soil of $CO_2$, and $0.29 \pm 0.01$ mmole/g dry soil of $CH_4$ over seven days of incubation. Compared to S-O-, the $SO_4^{2-}$ addition increased the carbon transfer to organic acids by 94% ($p$-value = 0.0003, t-test) and decreased the $CH_4$ production by 73% ($p$-value < 0.0001, t-test), and the $O_2$ exposure decreased the carbon transfer to organic acids by 76% ($p$-value = 0.0002, t-test), increased that to $CO_2$ by 70% ($p$-value < 0.0001, t-test), and eliminated the $CH_4$ production. Under the S-O- condition, $1.36 \pm 0.13$ mmole/g dry soil of electrons was transferred to organic acids, $0.19 \pm 0.01$ mmole/g dry soil to $H_2$, and $2.32 \pm 0.63$ mmole/g dry soil to $CH_4$. In comparison, the $SO_4^{2-}$ addition diverted $1.44 \pm 0.07$ mmole/g dry soil of electrons to $H_2S$ and decreased the electron transfer to $H_2$ by 40% ($p$-value = 0.0004, t-test), and the $O_2$ exposure decreased the electron transfer to $H_2$ by 55% ($p$-value = 0.001, t-test). The effects of the combined exposure to both $SO_4^{2-}$ and $O_2$ on the carbon and electron transfers were similar to the effects of the $O_2$ exposure only.

## $SO_4^{2-}$ and $O_2$ additions altered depolymerization of plant polysaccharides

The formation of hydrolysis products derived from plant polysaccharides, such as glucose, xylose, mannose, and galacturonic acid, was affected by exposure to $SO_4^{2-}$ and $O_2$ over time (Supplementary Fig. 1a – 1d). Under both anoxic and oxic conditions, the addition of $SO_4^{2-}$ slowed down the accumulation of glucose. This resulted in a 12% lower accumulation under anoxic conditions ($p$-value = 0.04, t-test) and a 14% reduced glucose accumulation ($p$-value = 0.02, t-test) under oxic conditions (Supplementary Fig. 1). Xylose reached its peak accumulation later under anoxic conditions compared to oxic conditions. The highest accumulation of xylose was observed under the S-O- condition, while its accumulation was relatively similar under the other three conditions. Mannose and galacturonic acid continuously accumulated under anoxic conditions. Their accumulation peaked between 16 to 23 days and then decreased under oxic conditions.

The metaproteomic analysis identified five key enzymes from species involved in the degradation of plant polysaccharides. These species had the highest proteome abundance under anoxic conditions. Pairwise comparisons of proteome richness and evenness of these species, between the S-O- condition and the S-O+ condition, as well as between the S+O+ condition and the S+O+ condition, revealed no significant changes under different oxic conditions, which suggests that the actual species composition

remained relatively stable across four conditions. A strong negative correlation (r = -0.70, $p$-value = 0.01, t-test) was observed between the total proteome abundance of plant polysaccharide-degrading microbes and the accumulation of $CO_2$ (Fig. 3a). Conversely, a weak positive correlation was observed between the total proteome abundance of these microbes and the accumulation of $CH_4$ (Fig. 3a).

The identified carbohydrate-active enzymes (CAZymes), including pectate lyase, beta-glucosidase, xylosidase, beta-galactosidase, and starch phosphorylase, showed the highest total abundance under the S-O- condition, and the lowest abundance under the S+O+ condition (Fig. 3b). This indicates that elevated $SO_4^{2-}$ and $O_2$ levels suppressed the activities of plant polysaccharide degradation.

Among the identified CAZymes, beta-glucosidase was detected across all conditions, with the highest abundance observed under the S+O- condition (fold change > 4.0, $q$-value < 0.007). Xylosidase, involved in xylan degradation, showed higher abundance under the S+O- condition (fold change > 3.2, $q$-value < 0.0001) (Supplementary Table 3), indicating enhanced cellulose and xylan degradation capacity under this condition. Beta-galactosidase was only detected under the S+O+ condition (Supplementary Table 3). This enzyme can release galactose from hemicellulose, which enters the glycolysis pathway after conversion into glucose 1-phosphate by glucuronate isomerase (UXA). The highest abundance of UXA proteins was detected under the S+O+ condition (fold change > 1.7, $q$-value < 0.0001) (Supplementary Table 3), suggesting enhanced hemicellulose utilization under this condition. These observations collectively demonstrate that changes in $SO_4^{2-}$ and $O_2$ levels altered the preference of the microbial community in degrading plant polysaccharides. Specifically, the enzymes enriched under oxic conditions use more complex structural substrates (e.g., hemicellulose) compared to those enriched under anoxic conditions (e.g., cellulose).

## $SO_4^{2-}$ and $O_2$ decreased methanogenesis and promoted methane oxidation

Under the S-O- condition, the microbial community continuously produced $CH_4$ ($0.29 \pm 0.007$ mmole/g dry soil) and $CO_2$ ($0.44 \pm 0.02$ mmole/g dry soil) throughout the experiment (Fig. 4a, b). The two-way ANOVA indicated a significant interaction between $SO_4^{2-}$ and $O_2$ on $CH_4$ accumulation ($F_{(1,8)} = 1590$, $p$-value < 0.0001). $CH_4$ release was reduced by 73% ($p$-value < 0.0001, t-test) under the S+O- condition, and by 97% ($p$-
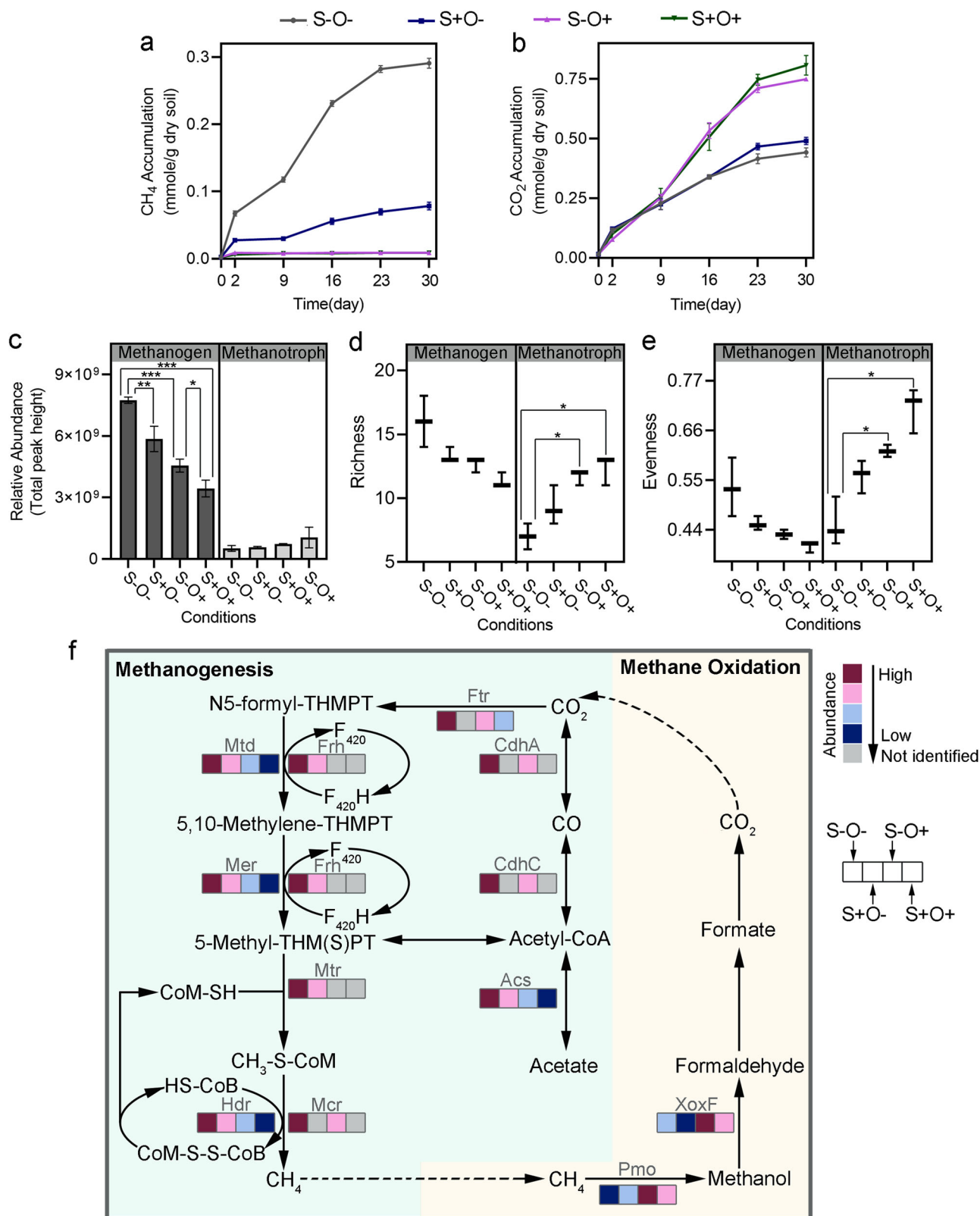
**Fig. 4 | Modulation of methane metabolism by $SO_4^{2-}$ and $O_2$ exposures.**
**a, b** Changes in molar mass of $CH_4$ **a** and $CO_2$ **b** under the four conditions, over a 30-day incubation. **c–e** Comparison of methanogens and methanotrophs in terms of relative abundance **c**, richness **d**, and evenness **e** under the four conditions. Relative abundance is quantified as the aggregate of protein abundances attributable to a specific species. **f** Schematic representation of methane metabolic pathways. The boxes in the pathway map, arranged from left to right, correspond to the S-O-, S+O-, S-O+ and S+O+ conditions. The color gradient from red to blue represents the relative abundance ranking of proteins among the four conditions, with red indicating the highest ranked relative abundance and blue the lowest. The gray color indicates proteins not detected by LC-MS/MS. Significant differences with p-values determined using Student's t-test, and adjusted for the false discovery rate, are marked by * for p-value < 0.05, ** for p-value < 0.01 and *** for p-value < 0.001. The error bars are defined as standard deviation.

**Table 1 | Accumulation of metabolic products in the microcosms under the four incubation conditions**

| Conditions | | | | |
|---|---|---|---|---|
| Metabolites (mmole/g dry soil) | S-O- | S+O- | S-O+ | S+O+ |
| Glucose | 0.023 ± 0.003 | 0.02 ± 0.002 | 0.02 ± 0.001 | 0.016 ± 0.001 |
| Xylose | 0.033 ± 0.001 | 0.023 ± 0.004 | 0.02 ± 0.002 | 0.02 ± 0.001 |
| Mannose | 0.008 ± 0.001 | 0.008 ± 0.001 | 0.011 ± 0.001 | 0.011 ± 0.001 |
| Galacturonic acid | 0.015 ± 0.003 | 0.016 ± 0.002 | 0.019 ± 0.001 | 0.015 ± 0.001 |
| $H_2$ | 0.096 ± 0.005 | 0.058 ± 0.003 | 0.044 ± 0.009 | 0.037 ± 0.001 |
| $CO_2$ | 0.44 ± 0.02 | 0.49 ± 0.02 | 0.75 ± 0.008 | 0.81 ± 0.04 |
| $CH_4$ | 0.29 ± 0.007 | 0.079 ± 0.006 | 0.009 ± 0.001 | 0.008 ± 0.001 |
| $H_2S$ | 0 | 0.18 ± 0.008 | 0 | 0.003 ± 0.001 |
| Acetate | 0.11 ± 0.012 | 0.21 ± 0.013 | 0.021 ± 0.002 | 0.022 ± 0.004 |
| Lactate | 0.01 ± 0.002 | 0.037 ± 0.004 | 0.012 ± 0.002 | 0.013 ± 0.002 |
| Butyrate | 0.02 ± 0.002 | 0.012 ± 0.004 | 0 | 0 |

value < 0.000, t-test) under the S-O+ condition (Fig. 4a and Table 1), highlighting the higher sensitivity of $CH_4$ accumulation to $O_2$ than to $SO_4^{2-}$. However, the same analysis showed no significant interaction between $SO_4^{2-}$ and $O_2$ (F (1, 8) = 0.1, $p$-value = 0.75). The main effects were observed, $CO_2$ accumulation increased by 11% higher under the S+O- condition ($p$-value = 0.03, t-test), by 70% higher under the S-O+ condition ($p$-value < 0.0001, t-test), and by 83% higher under the S+O+ condition ($p$-value = 0.0002, t-test), compared to the S-O- condition (Fig. 4b), suggesting an additive effect of $SO_4^{2-}$ and $O_2$ on $CO_2$ accumulations.

Metaproteomic analysis identified 634 proteins from methanogens (Supplementary Table 1). These methanogens showed the highest proteome abundance under the S-O- condition, constituting 22% of the total metaproteome (Supplementary Table 1). The addition of $SO_4^{2-}$ and $O_2$, either individually or in combination, led to a reduction in the proteome abundance ($p$-value < 0.0001, one-way ANOVA), richness ($p$-value = 0.005, one-way ANOVA), and evenness ($p$-value = 0.008, one-way ANOVA) of methanogenic populations (Fig. 4c–e). Furthermore, strong positive correlations were observed between the $CH_4$ accumulation and the proteome abundance (r = 0.9, $p$-value < 0.0001, t-test), richness (r = 0.9, $p$-value = 0.0001, t-test), as well as evenness (r = 0.8, $p$-value = 0.002, t-test) of methanogens (Supplementary Fig. 2). In summary, the observed relationships among $SO_4^{2-}$ and $O_2$ availability, $CH_4$ accumulation, and the composition of methanogen populations could serve as diagnostics for more predictive climate modeling.

Metaproteomics revealed significant suppression of both hydrogenotrophic and acetoclastic methanogenesis by $SO_4^{2-}$ and $O_2$. Many marker proteins involved in methanogenesis, including methyl-coenzyme M reductase (Mcr), 5,10-methylenetetrahydromethanopterin reductase (Mer), tetrahydromethanopterin S-methyltransferase (Mtr), acetyl-CoA decarbonylase/synthetase (CdhA) and methylenetetrahydromethanopterin dehydrogenase (Mtd) were most abundant under S-O- condition (Fig. 4f and Table 2). The addition of $SO_4^{2-}$ and $O_2$, either individually or in combination, led to a significant decrease in the abundance of these proteins (Fig. 4f). This decrease coincided with the decrease in $CH_4$ emissions observed when exposed to $SO_4^{2-}$ and $O_2$ stressors (Fig. 4a).

Furthermore, the $SO_4^{2-}$ and $O_2$ exposures suppressed hydrogenotrophic methanogenesis much more than acetoclastic methanogenesis. Specifically, after $SO_4^{2-}$ addition to the anoxic sediment, the abundance of acetyl-CoA decarbonylase/synthetase essential for acetoclastic methanogenesis, decreased by 1.2-fold ($q$-value = 0.0001). And there was a more pronounced decrease in proteins for hydrogenotrophic methanogenesis (Fig. 4f, Table 2), including a 3.4-fold decrease of the 5,10-methylenetetrahydromethanopterin reductase ($q$-value = 0.003) and a 5.8-fold decrease

of the tetrahydromethanopterin S-methyltransferase ($q$-value < 0.0001). This indicated a stronger suppression of hydrogenotrophic methanogenesis by $SO_4^{2-}$. Under S-O+ condition, we observed a decrease in proteins for both the acetoclastic and hydrogenotrophic pathways of methanogenesis when compared to S-O- condition. In the acetoclastic pathway, there was a 2.6-fold decrease in acetyl-CoA synthetase (Acs) ($q$-value = 0.01) and a 2.1-fold decrease in methyl-coenzyme M reductase ($q$-value < 0.0001) (Fig. 4f, Table 2). In the hydrogenotrophic pathway, there was a 7.0-fold decrease in the methylenetetrahydromethanopterin dehydrogenase ($q$-value < 0.0001) and a 3.1-fold decrease in methyl-coenzyme M reductase ($q$-value = 0.02). Similarly, under S+O+ condition, compared to the S+O- condition, there was a more substantial decrease in key enzymes associated with hydrogenotrophic methanogenesis, including a 9.2-fold decrease in 5,10-methylenetetrahydromethanopterin reductase ($q$-value < 0.0001) and a 5.0-fold decrease in tetrahydromethanopterin S-methyltransferase ($q$-value < 0.01), compared to a 1.5-fold decrease in acetyl-CoA decarbonylase/synthetase ($q$-value = 0.006). These results highlight that $O_2$ had a greater suppression of hydrogenotrophic methanogenesis than acetoclastic methanogenesis. Moreover, compared to the S-O- condition, under S+O+ condition, the abundance of methyl-coenzyme M reductase decreased by 1.7-fold ($q$-value = 0.01), and the abundance of tetrahydromethanopterin S-methyltransferase decreased by 8.7-fold ($q$-value < 0.0001). This suggests that the combined addition of $SO_4^{2-}$ and $O_2$ had a more significant impact on hydrogenotrophic methanogenesis compared to acetoclastic methanogenesis.

In addition, metaproteomics identified 208 proteins from methanotrophs (Supplementary Table 1). Under the S+O+ condition, methanotrophs showed the highest richness ($p$-value = 0.0001, one-way ANOVA), and evenness ($p$-value = 0.0004, one-way ANOVA) (Fig. 4c–e). Moreover, significant negative correlations were found among the $CH_4$ accumulation and proteome abundance (r = -0.7, $p$-value = 0.02, t-test), richness (r = -0.9, $p$-value < 0.0001, t-test), and evenness (r = -0.8, $p$-value = 0.002, t-test) of active methanotrophs (Supplementary Fig. 2).

Key enzymes involved in methane oxidation, including methane/ammonia monooxygenase (Pmo) and lanthanide-dependent methanol dehydrogenase (XoxF), showed distinct responses to elevated $SO_4^{2-}$ and $O_2$ (Fig. 4f and Table 2). Under the anoxic condition, $SO_4^{2-}$ addition increased the abundance of methane/ammonia monooxygenase and lanthanide-dependent methanol dehydrogenase by 2.3-fold ($q$-value < 0.0001) and 1.4-fold ($q$-value = 0.0002), respectively. However, under the oxic conditions, $SO_4^{2-}$ addition decreased the abundance of lanthanide-dependent methanol dehydrogenase by 1.7-fold ($q$-value = 0.005). Oxygen addition led to an increase in the abundance of methane/ammonia monooxygenase and lanthanide-dependent methanol dehydrogenase by 3.9-fold ($q$-value < 0.0001) and 2.5-fold ($q$-value = 0.006), respectively, under the non-sulfate-addition condition. Under the sulfate-addition condition, their abundance increased by 1.7-fold ($q$-value = 0.005) and 3.0-fold ($q$-value < 0.0001), respectively. Furthermore, when compared to S-O- condition, the abundance of methane/ammonia monooxygenase and lanthanide-dependent methanol dehydrogenase increased by 4.2-fold ($q$-value < 0.0001) and by 3.9-fold ($q$-value = 0.001) under S+O+ condition (Fig. 4f, Table 2).

## $SO_4^{2-}$ and $O_2$ additions changed metabolic behaviors of sulfate-reducing bacteria

Under the sulfate-limited conditions, some sulfate-reducing bacteria (SRB) function as syntrophic oxidizers, metabolizing lactate to produce acetate, $H_2$, and $CO_2$. With added $SO_4^{2-}$, SRB may oxidize lactate to acetate and $CO_2$ and concurrently reduce $SO_4^{2-}$ to $H_2S$[28]. Two-way ANOVA indicated a significant interaction between $SO_4^{2-}$ and $O_2$ on lactate accumulation (F (1,8) = 66.51, $p$-value < 0.0001), with significant main effects of $SO_4^{2-}$ (F (1, 8) = 55.4, $p$-value < 0.0001) and $O_2$ (F (1, 8) = 74.76, $p$-value < 0.0001). Under the S-O- condition, lactate substantially accumulated, reaching its peak of 0.033 ± 0.004 mmole/g dry soil on day 9, and then decreased to 0.018 ± 0.002 mmole/g dry soil over the next 7 days. Under the S+O- condition, lactate accumulation continually increased, reaching

**Table 2 | Key proteins in methane metabolism and sulfate reduction pathways**

| Processes | Enzymes | Symbol | Comparison | | | | |
|---|---|---|---|---|---|---|---|
| | | | S-O- vs. S+O- | S-O+ vs S+O+ | S-O- vs. S-O+ | S+O- vs. S+O+ | S-O- vs. S+O+ |
| | | | Fold Change (*padj*) | Fold Change (*padj*) | Fold Change (*padj*) | Fold Change (*padj*) | Fold Change (*padj*) |
| | methyl-coenzyme M reductase | Mcr | — | — | 3.1 (*) ▼ | — | — |
| Hydrogenotrophic Methanogenesis | 5,10-methylenetetrahydromethanopterin reductase | Mer | 3.4 (**) ▼ | — | — | 9.2 (***) ▼ | — |
| | tetrahydromethanopterin S-methyltransferase | Mtr | 5.8 (***) ▼ | — | — | 5.0 (*) ▼ | 8.7 (***) ▼ |
| | methylenetetrahydromethanopterin dehydrogenase | Mtd | — | — | 7.0 (***) ▼ | — | — |
| Acetoclastic Methanogenesis | acetyl-CoA decarbonylase/synthetase | CdhA | 1.2 (***) ▼ | — | | | |
| | acetyl-CoA synthetase | Acs | — | — | 2.6 (*) ▼ | 1.5 (**) ▼ | — |
| | methyl-coenzyme M reductase | Mcr | — | — | 2.1 (***) ▼ | - | 1.7 (*) ▼ |
| Methane Oxidation | methane/ammonia monooxygenase | Pmo | 2.3 (***) ▲ | — | 3.9 (***) ▲ | 1.7 (**) ▲ | 3.9 (**) ▲ |
| | lanthanide-dependent methanol dehydrogenase | XoxF | 1.4 (***) ▲ | 1.7 (**) ▲ | 2.5 (**) ▲ | 3.0 (***) ▲ | 4.2 (***) ▲ |
| Sulfate Reduction | pyruvate ferredoxin oxidoreductase | Por | 8.0 (***) ▲ | 1.8 (**) ▲ | 1.4 (***) ▼ | | 5.7 (***) |
| | acetyl-CoA synthetase | Acs | 5.3 (***) ▲ | 2.4 (***) ▲ | 3.2 (***) ▼ | 2.0 (***) ▼ | — |
| | sulfate adenylyltransferase | Sat | 1.4 (**) ▲ | 2.8 (***) ▲ | 2.3 (**) ▼ | 1.2 (*) ▼ | 1.2 (***) ▼ |
| | adenylylsulfate reductase | Apr | 1.8 (***) ▲ | - | 1.3 (**) ▼ | 1.5 (**) ▼ | 1.2 (**) ▼ |
| | dissimilatory sulfite reductase | Dsr | 1.5 (**) ▲ | 1.6 (***) ▲ | 1.4 (***) ▼ | — | — |

▲ significant increase, ▼ significant decrease, - no significant changes were observed.

\* for padj < 0.05, ** for padj < 0.01 and *** for padj < 0.001.

The enzymes listed in the table have shown significant changes in at least one of the five comparison groups.

$0.037 \pm 0.004$ mmole/g dry soil at the end of incubation. Under oxic conditions, lactate accumulation remained consistently low at less than $0.012 \pm 0.004$ mmole/g dry soil over 30 days (Fig. 5a). Similarly, the two-way ANOVA for $H_2S$ accumulation revealed a significant interaction between $SO_4^{2-}$ and $O_2$ ($F(1, 8) = 1222$, $p$-value < 0.0001), with significant main effects for both $SO_4^{2-}$ and $O_2$. Specifically, a substantial accumulation of $H_2S$ ($0.18 \pm 0.008$ mmole/g dry soil) was observed under the S+O- condition, while only trace amounts of $H_2S$ ($0.003 \pm 0.0002$ mmole/g dry soil) were detected under the S+O+ condition (Fig. 5b).

Metaproteomics identified a total of 145 proteins from SRB species, with the highest SRB proteome abundance observed under S+O- condition (fold change > 1.3, $p$-value < 0.006, t-test) (Fig. 5c, Supplementary Table 1). $SO_4^{2-}$ addition enhanced the activities of both lactate oxidation and dissimilatory sulfate reduction within this community (Fig. 5d–f and Table 2). In the lactate oxidation pathway, $SO_4^{2-}$ addition resulted in an 8.0-fold increase in the abundance of pyruvate ferredoxin oxidoreductase (Por) ($q$-value < 0.0001) and a 5.3-fold increase in acetyl-CoA synthetase ($q$-value < 0.0001). In the dissimilatory sulfate reduction pathway, the abundance of adenylylsulfate reductase (Apr) increased by 1.8-fold ($q$-value < 0.0001), sulfate adenylyltransferase (Sat) increased by 1.4-fold ($q$-value = 0.002), and dissimilatory sulfite reductase (Dsr) increased by 1.5-fold ($q$-value = 0.005) following $SO_4^{2-}$ addition (Fig. 5f, Table 2).

Oxygen addition significantly suppressed the activities of lactate oxidation and dissimilatory sulfate reduction. The response of key proteins in both pathways to $O_2$ varied with the availability of $SO_4^{2-}$. In the lactate oxidation pathway, the reduction in the abundance of acetyl-CoA synthetase was more significant when comparing S-O- to S-O+ condition (2.6-fold decrease, $q$-value = 0.01), than when comparing S+O- to the S+O+ condition (1.5-fold decrease, $q$-value = 0.006). A 1.4-fold reduction ($q$-value < 0.0001) in pyruvate ferredoxin oxidoreductase was observed only when comparing S-O- to S-O+ condition, suggesting that $O_2$ showed a stronger suppressive effect under the sulfate-sufficient condition. Conversely, in the dissimilatory sulfate reduction pathway, the suppressive effect of $O_2$ was intensified under sulfate-limited conditions, as indicated by a

larger decrease in the abundance of sulfate adenylyltransferase when comparing S-O- to S-O+ condition (2.3-fold decrease, $q$-value = 0.007), than when comparing S+O- to S+O+ condition (1.2-fold decrease, $q$-value = 0.01). Additionally, a 1.4-fold ($q$-value = 0.0001) decrease in the abundance of dissimilatory sulfate reductase was only observed when comparing S-O- to S-O+ condition (Fig. 5f, Table 2) and no significant change when comparing S+O- to S+O+ condition.

Furthermore, metaproteomics analysis identified a total of 779 proteins from sulfide/sulfur-oxidizing bacteria (SOB), with the highest SOB proteome abundance observed under S+O+ condition (Fig. 5c and Supplementary Table 1). The proteome abundance of SOBs was negatively correlated with the $CH_4$ accumulation ($r = -0.7$, $p$-value = 0.01, t-test), while the evenness of SOBs showed a positive correlation with the $CH_4$ accumulation ($r = 0.8$, $p$-value = 0.0006, t-test) (Supplementary Fig. 2).

## Modeling of carbon and energy flow through the microbial communities

A stoichiometric model was constructed to model the fluxes through the primary carbon metabolism and energy conservation pathways among the predominant microbial guilds in the wetland communities. The overall model comprised nine reactions, including aerobic heterotrophy, lactate fermentation, hydrogenic acetogenesis, sulfidogenic lactate oxidation, sulfidogenic hydrogen oxidation, hydrogenotrophic methanogenesis, acetoclastic methanogenesis, methane oxidation, and butyrate production (Supplementary Fig. 3). The fluxes of these reactions were fitted to the cumulative amounts of acetate, lactate, butyrate, $H_2$, $CO_2$, $CH_4$, and $H_2S$ produced or consumed over the 30 days of incubation. The correlation coefficient $R^2$, exceeded 0.9 in all four conditions (Supplementary Fig. 4). The consistency between the experimental data and the modeling results indicated a plausible estimation of the carbon and energy flows.

Under the S-O- condition, the primary reactions involved were hydrogenic acetogenesis, hydrogenotrophic methanogenesis, and acetoclastic methanogenesis. $SO_4^{2-}$ addition significantly increased the flux from 0 to $0.33 \pm 0.005$ mmole/g dry soil through sulfidogenic hydrogen oxidation
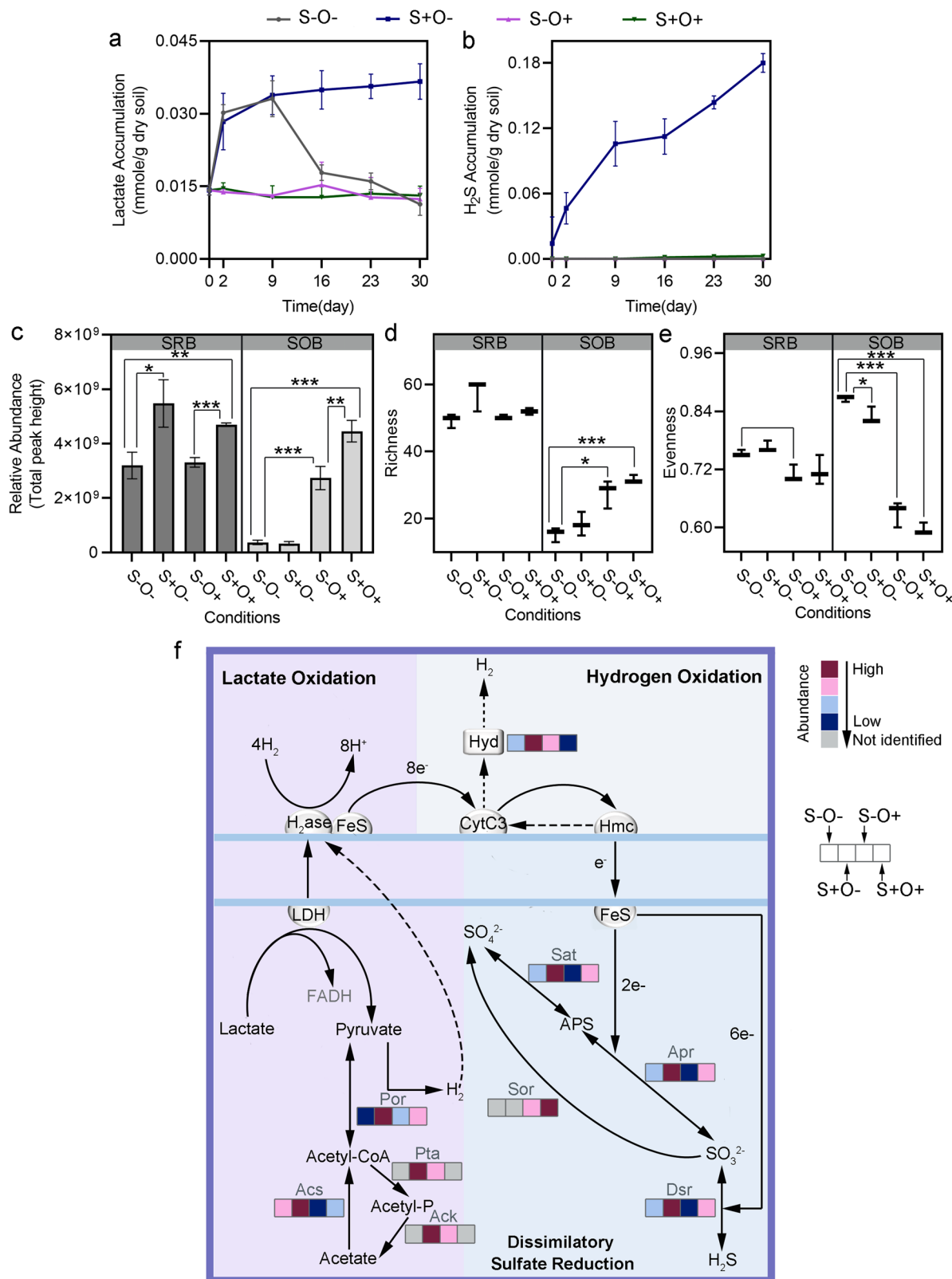
**Fig. 5 | Effects of SO$_4^{2-}$ and O$_2$ exposures on sulfate reduction and sulfite/sulfide oxidation processes. a, b** Changes in molar mass of lactate **a** and H$_2$S **b** over the 30 days of incubation. **c–e** Relative abundances **c**, richness **d**, and evenness **e** of sulfate-reducing bacteria (SRB) and sulfide/sulfur-oxidizing bacteria (SOB). Significant differences with $p$-values determined using Student's t-test, and adjusted for the false discovery rate, are marked by * for $p$-value < 0.05, ** for $p$-value < 0.01 and *** for $p$-value < 0.001. **f** Sulfur metabolism pathways. The boxes in the pathway map, arranged from left to right, correspond to the S-O-, S+O-, S-O+ and S+O+ conditions. The color gradient from red to blue represents the relative abundance ranking of proteins among the four conditions, with red indicating the highest ranked relative abundance and blue the lowest. The gray color indicates proteins not detected by LC-MS/MS. The error bars are defined as standard deviation.
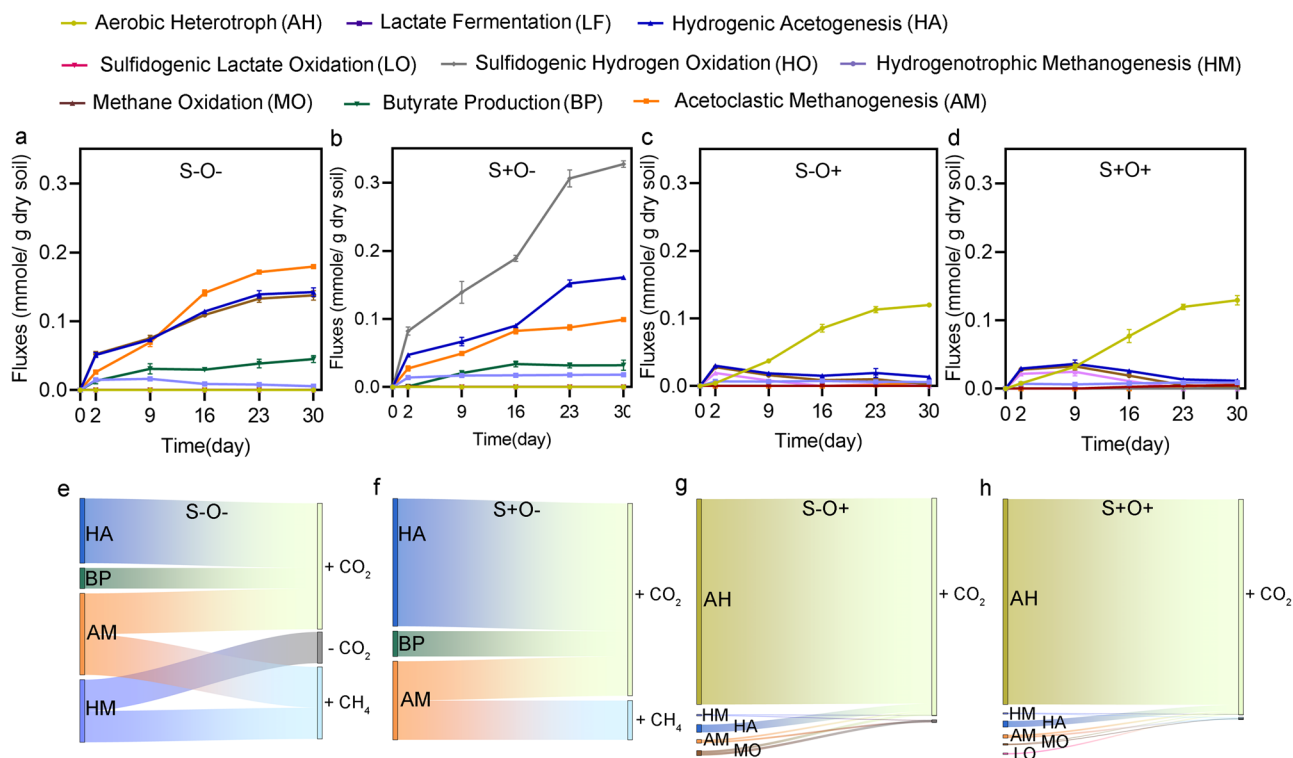
**Fig. 6 | Stoichiometric modeling of the wetland microbial community. a–d** fluxes of the key reactions under four experimental conditions. **e–h** Production (+) and consumption (-) of $CO_2$ and $CH_4$ by these reactions. The error bars are defined as standard deviation.

(Fig. 6a, b). This observation was consistent with the increased abundance of functional proteins, including sulfate adenylyltransferase (1.4-fold, $q$-value = 0.002), adenylylsulfate reductase (1.8-fold, $q$-value < 0.001) and dissimilatory sulfate reductase (1.5-fold, $q$-value = 0.001) in the dissimilatory sulfate reduction pathway (Fig. 5c). Furthermore, $SO_4^{2-}$ addition halted hydrogenotrophic methanogenesis and significantly reduced the flux by 1.7- folds through acetoclastic methanogenesis ($p$-value = 0.0014, Wald type II $\chi^2$ tests) (Fig. 6b). These reductions were supported by the fact that the abundance of functional proteins for hydrogenotrophic methanogenesis decreased much more than for acetoclastic methanogenesis. Under the two oxic conditions, the dominant reaction shifted to aerobic heterotrophy. The fluxes through dominant reactions observed under anoxic conditions were consistently lower than oxic conditions, such as hydrogenic acetogenesis (fold change > 3.9, $p$-value = 0.000, Wald type II $\chi^2$ tests), hydrogenotrophic methanogenesis (fold change = 6.0, $p$-value = 0.004, Wald type II $\chi^2$ tests), and acetoclastic methanogenesis (fold change > 35.4, $p$-value = 0.0003, Wald type II $\chi^2$ tests). Moreover, $O_2$ also eliminated sulfidogenic hydrogen oxidation and butyrate production (Fig. 6c, d). Under S+O+ condition, sulfidogenic lactate oxidation replaced sulfidogenic hydrogen oxidation for sulfate reduction compared to S+O- condition (Fig. 6b, d). These findings indicate that the addition of $SO_4^{2-}$ and $O_2$ restructured the carbon flows across the metabolic network of the wetland community.

The models estimated the contributions of each reaction to the $CO_2$ and $CH_4$ accumulations. Under S-O- condition – where $CO_2$ accumulation was lowest – it was estimated 51% of $CO_2$ was derived from hydrogenic acetogenesis (0.28 ± 0.01 mmole/g dry soil), 32% from acetoclastic methanogenesis (0.18 ± 0.002 mmole/g dry soil), and 17% from butyrate production (0.091 ± 0.01 mmole/g dry soil). Additionally, 0.14 ± 0.008 mmole/ g dry soil $CO_2$ was used for hydrogenotrophic methanogenesis to produce $CH_4$. $SO_4^{2-}$ addition reduced the contributions of butyrate production (0.064 ± 0.014 mmole/g dry soil) and acetoclastic methanogenesis (0.099 ± 0.002 mmole/g dry soil) to $CO_2$ accumulation by 31% and 45%, respectively. However, the contribution of $CO_2$ accumulation from hydrogenotrophic acetogenesis increased by 13%, and no flux was detected

from hydrogenotrophic methanogenesis using $CO_2$ to produce $CH_4$. These overall changes resulted in a 16% increase in total $CO_2$ accumulation. The highest $CH_4$ accumulation was observed under S-O- condition, with acetoclastic methanogenesis contributing 56.6% (0.18 ± 0.002 mmole/g dry soil) and hydrogenotrophic methanogenesis contributing 43.4% (0.14 ± 0.008 mmole/g dry soil) (Fig. 6e). Under the S+O- condition, only acetoclastic methanogenesis contributed to $CH_4$ accumulation, and the total $CH_4$ accumulation decreased by 69% compared to the S-O- condition (Fig. 6f). Under the two oxic conditions, aerobic heterotrophs contributed 94% and 96% of the $CO_2$ produced under non-sulfate addition and sulfate addition conditions, respectively (Fig. 6g, h).

## Discussion

Climate change will result in increased hydrological challenges to wetlands, including seawater intrusion and changing regional regimes of drought and flooding. These stressors lead to recurrent perturbations in wetland microbial communities, primarily due to elevated $O_2$ during periods of drought and elevated $SO_4^{2-}$ from seawater intrusion[22,29]. Our findings demonstrated that the addition of $SO_4^{2-}$ and $O_2$ diminished $CH_4$ emissions and increased $CO_2$ emissions, which is consistent with observations in natural wetland ecosystems exposed to increased seawater and $O_2$[1,30,31]. However, it remains challenging in natural wetland soil to determine how $SO_4^{2-}$ and $O_2$ shape microbial processes that ultimately impact $CH_4$ and $CO_2$ emissions[32,33]. In this study, we developed a conceptual food web connecting the metabolic activities of key microbial populations to $CH_4$ and $CO_2$ emissions, under the perturbation of elevated $SO_4^{2-}$ and $O_2$ (Fig. 7). Our findings indicated that elevated availabilities of $SO_4^{2-}$ and $O_2$ changed the compositions of functional guilds and their metabolic activities, including plant polymer breakdown, methane production and oxidation, as well as sulfide/sulfur oxidation. Elevated $SO_4^{2-}$ reduced $CH_4$ emission by 3.7-fold and increased $CO_2$ emission by 1.1-fold. Exposure to $O_2$ resulted in a 33.3-fold decrease in $CH_4$ emission and only a 1.7-fold increase in $CO_2$ emission. Because the

**Fig. 7 | Conceptual food web responding to $SO_4^{2-}$ and $O_2$ perturbations.** The S-O- condition serves as the baseline. Circle size corresponds to the relative abundance of marker proteins within the reaction, with larger circles indicating higher abundance, and smaller circles denoting lower abundance. Numbers alongside circles indicate the fold change in metabolic fluxes as inferred from stoichiometric models relative to the control. Edge thickness represents the magnitude of fluxes that consume or produce metabolites. Dashed lines indicate fluxes for nearly eliminated hydrogenotrophic methanogenesis post-treatment. Statistical significance was assessed by Wald type II $\chi^2$ tests, with $p$-values adjusted for the false discovery rate indicated by: *** $p < 0.001$, ** $p < 0.01$, * $p < 0.05$.
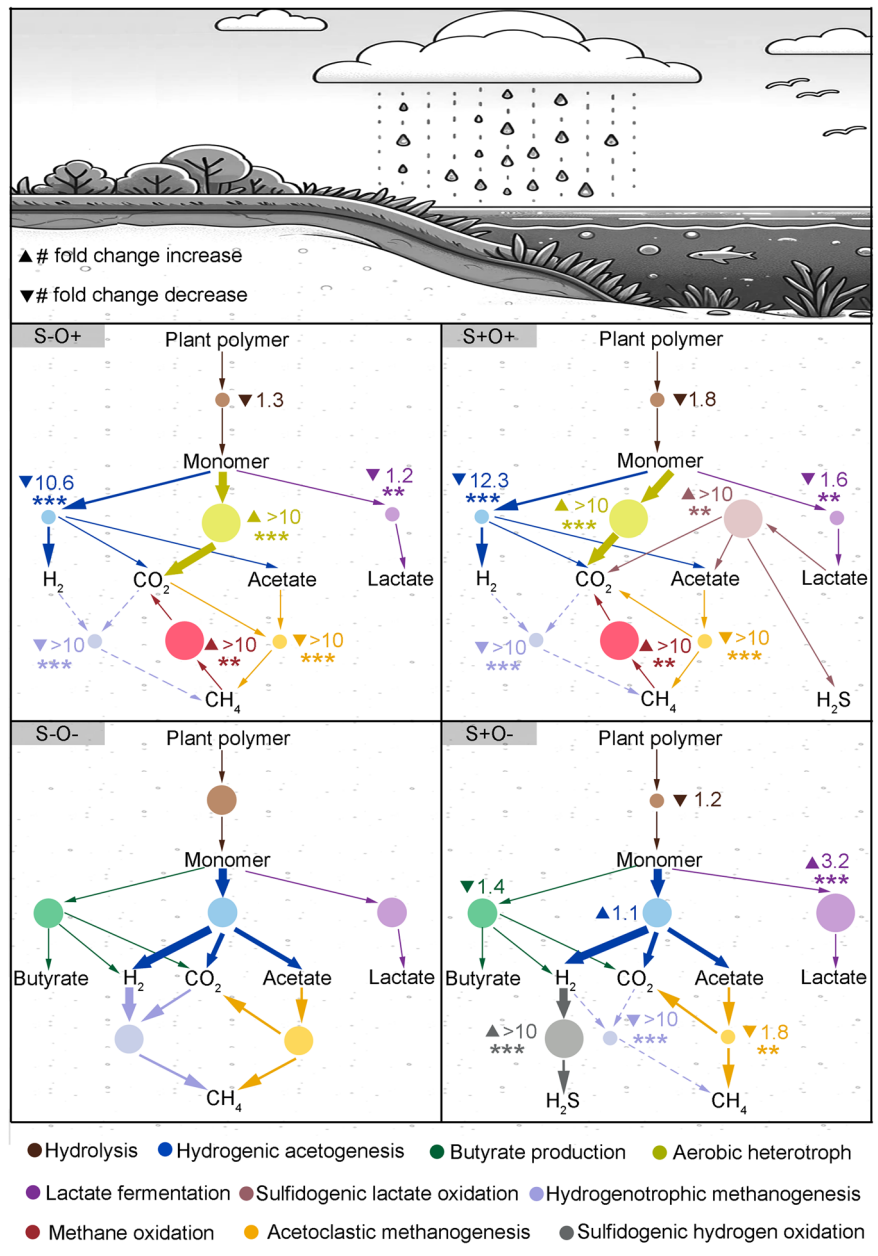


warming effect of $CH_4$ is approximately 28-36 times greater than that of $CO_2$[34], the elevated $SO_4^{2-}$ and $O_2$ exposures may reduce the overall warming effect of gas emissions from wetlands.

The reduction in the $CH_4$ production by $SO_4^{2-}$ exposure was attributed primarily to the sharp decrease in $H_2$ available for hydrogenotrophic methanogenesis and acetate needed for acetoclastic methanogenesis. Notably, hydrogenotrophic methanogenesis appeared to be more sensitive to elevated $SO_4^{2-}$ compared to acetoclastic methanogenesis. This sensitivity is rooted in the thermodynamic basis of competition for $H_2$ and carbon by methanogenic consortia and SRB, as hydrogenotrophic sulfate reduction is more energetically favorable than either hydrogenotrophic methanogenesis or acetoclastic methanogenesis[22,35,36]. Even under oxic conditions, $SO_4^{2-}$ addition facilitated the co-existence of SOB and SRB. Oxygen consumed by sulfide-oxidizing SOB fosters the growth of anaerobic sulfide-generating SRB. In contrast, acetoclastic methanogens do not directly compete with SRB, as most SRBs have an incomplete TCA cycle, which prevents them from completing the oxidation of acetate to $CO_2$[37,38]. In addition, our results indicated that a key factor contributing to the increase in $CO_2$ emission due to the addition of $SO_4^{2-}$ is the inhibition of hydrogenotrophic

methanogenesis, which consumes $CO_2$. $SO_4^{2-}$ addition reorganized carbon fluxes through the community due to SRB outcompeting hydrogenotrophic methanogens, in turn driving accumulation of short-chain fatty acids and increasing $CO_2$ emissions.

$O_2$ suppressed both hydrogenotrophic methanogenesis and acetoclastic methanogenesis. In the absence of $SO_4^{2-}$, elevated $O_2$ suppressed reactions that produce $H_2$, such as hydrogenic acetogenesis. The decreased $H_2$ production constrained the hydrogenotrophic methanogenesis[39]. Under the sulfate addition conditions, the introduction of $O_2$ was found to enhance the consumption of $H_2S$ by SOB. Consequently, this promoted $H_2$ uptake by sulfate reduction and intensified the competition between hydrogenotrophic methanogens and SRB[38]. The proteomic abundances of carbohydrate degradation enzymes also indicated that $O_2$ altered the preference for the degradation of plant polysaccharides. Exposure to $O_2$ favored microbial communities that hydrolyze polysaccharides with more complex structures. Upon recovery from oxic conditions, this may lead to prolonged release of $CO_2$[24].

Approximately 80% of the studies investigating the impact of anthropogenic pressures on ecosystem functions have primarily focused on

analyzing the effect of individual stressors in isolation[40,41]. However, climate change may introduce many co-occurring stressors, which need to be investigated in combination. In this study, we found an antagonistic interaction between the effects of sulfate and $O_2$ on $CH_4$ and $CO_2$ emissions, where the reduction in $CH_4$ accumulation and the increase in $CO_2$ resulting from the combined treatment of $SO_4^{2-}$ and $O_2$ was less pronounced compared to the sum of individual effects. This non-additive effect can be attributed to the high functional redundancy stemming from extraordinarily diverse functional guilds in soils[41–43]. Furthermore, both $SO_4^{2-}$ and $O_2$ affect certain metabolic processes in a similar manner. For instance, elevated levels of either $SO_4^{2-}$ or $O_2$ nearly completely halted hydrogenotrophic methanogenesis, resulting in a reduction in $CH_4$ accumulation. Therefore, when $SO_4^{2-}$ and $O_2$ exposures are combined, the observed methanogenesis decrease is not additive.

In this study, we generated a functional understanding of the decreased $CH_4$ and increased $CO_2$ emissions in wetland microcosms subjected to $SO_4^{2-}$ and $O_2$ pressure by integrating geochemical analysis, proteogenomics, and stoichiometric modeling. The geochemical analysis quantified the end-products' accumulation levels and the intermediates' standing levels in the metabolic network, which were used by the stoichiometric modeling to estimate the flux rates across key metabolic processes under different conditions. Many of the changes in the estimated flux rates were supported by the concordant changes in the protein abundances of enzymes involved in those metabolic processes. The obtained results may enable climate models to better estimate greenhouse gas emissions under changing environmental conditions.

## Methods

### Sampling and soil microcosm set up

Triplicate soil samples were collected from a seasonally flooded urban freshwater wetland connected to Lake Washington in Seattle, WA, USA (Coordinates: 47.642196ºN, -122.296236ºW) in May 2022 using a soil core sampler with 2" x 6" plastic liners (AMS, Inc., American Falls, ID). The core sampler was forced approximately 60 cm into the sediment bed with a slide hammer to cut roots and other plant material. The three replicate soil cores were collected approximately one meter apart from each other, avoiding large tree branches or roots. The broader location was selected based on its variably submerged nature, with the water table generally being below the surface during the fall and winter months and above the surface during the spring and summer months. At the time of sampling, the water table was above the soil surface and the soil was completely saturated with water. The cores were sealed air-tight upon removal from the natural habitat, to protect the redox state of samples. Samples were then transported to the lab on ice, for immediate processing.

Microcosms were set up by filling 160 mL bottles with 40 g fresh sediment soil slurry in an anaerobic chamber. The chamber gas contained $N_2$ : $H_2$ (97:3). All bottles were preincubated for five days at room temperature and then incubated at 30 °C for 30 days. Soil microcosms were divided into four groups, with each group receiving specific treatments every two days: anoxic non-sulfate-addition, anoxic sulfate-addition (resulting in a final $SO_4^{2-}$ concentration of approximately 7.2 mM), oxic non-sulfate-addition (where half of the gas phase was replaced with sterile air), and oxic sulfate-addition, which was treated with both $SO_4^{2-}$ and sterile air. Sampling was conducted on days 2, 9, 16, 23, and 30, with each group sacrificing three bottles for sampling at the indicated time points. During sampling, 10 mL of gas phase products were collected in vacuumed Labco exetainer gas vails for later analysis. Then 10 ml of PBS buffer was injected into the bottle, and shaken at 200 rpm for 10 min, after which 10 ml of well-shaken culture liquid was sampled, and stored at -80 °C for subsequent analysis.

### Chemical analysis

Headspace pressure was measured using a pressure gauge (Cole Parmer SK-68900-24) before sampling. pH measurements were taken immediately after sampling. Analysis of $H_2$, $CO_2$ and $CH_4$ was carried out using a gas chromatograph (GC-8A, Shimadzu, Japan). $H_2S$ in the gas phase was measured

by an $H_2S$ monitor (Forensics, FD-103-H2S, US), the $H_2S$ dissolved in slurry was calculated based on the pH and the amount of $H_2S$ in the gas phase. Absolute gas composition was calculated with the ideal gas law. The soluble sugars (glucose, xylose, mannose and galacturonic acid) and fermentation products (acetate, lactate, and butyrate) in the slurry were analyzed by high-performance liquid chromatography (HPLC) as reported previously[44]. The metabolic measurements were standardized using the gram of dry soil at the endpoint, which constitutes 22.9 ± 0.1% of soil slurry.

### DNA extraction and metagenomic sequencing

Only the initial soils from the field were sequenced using metagenomic analysis. The total DNA in the triplicate field soil samples was extracted using the PowerMaxSoil DNA isolation kit as described previously[45]. Metagenomic library preparation and DNA sequencing were performed at the Joint Genome Institute. The metagenomic libraries were prepared for sequencing using 2 × 151-bp lanes on the Illumina NovaSeq S4 platform. A total of 404,050,411 ± 23,970,278 sequence reads were obtained.

### Metagenomic data processing

Metagenomic reads were preprocessed using BBTools for removing adaptors, trimming reads, and sequencing error correction[46]. The pre-processed reads from three replicates were co-assembled into a combined metagenome with SPAdes v3.15.5[47], A total of 857,101 scaffolds with a length > 1 kbp were retained. The total length and L50 of the assembly were 1,939,450,947 bp and 2420 bp, respectively. The percentage of sequencing reads mapped onto the scaffolds is 87%. Genes were called from these retained scaffolds using the Prodigal algorithm[48]. A total of 26,768,938 genes were identified. Gene functions were annotated using Kofamscan[49]. Taxonomic classification was carried out at the scaffold level using Kaiju, based on reference species in the NCBI RefSeq[50]. Metagenome-assembled genomes (MAGs) were obtained using MetaBAT v2.12.1 with default parameters[51]. The quality of MAGs was estimated using CheckM v1.1.2. The MAGs obtained were classified into high-quality MAGs with completeness > = 50% and contamination < 5%. The taxonomy classifications of high-quality MAGs were inferred using GTDB-Tk v2.3.2[52].

### Metaproteomics measurement

Soil cultures at the end of the experiment were analyzed by metaproteomics. Proteins were extracted as described previously. Briefly, soil samples were suspended in lysis buffer (containing 10 mM tris-HCl, 4% SDS and 10 mm dithiothreitol), boiled for 5 min and further disrupted by sonication for a 2 min 10% pulse 5 times. The supernatant was collected by centrifugation at 14,000 g for 10 min. Proteins were then precipitated by TCA (trichloroacetic acid) overnight and pelleted by centrifugation. Protein pellets were washed with ice-cold acetone three times and resuspended in guanidine buffer. Protein concentrations were quantified by Bicinchoninic Acid Assay. Twenty mg samples of proteins were processed using FASP (filter-aided sample preparation) and digested by Trypsin/LysC mixture. Each sample was analyzed using 2D-LC-MS/MS (two-dimensional liquid chromatography-tandem mass spectrometry) on an Orbitrap Fusion Tribrid mass spectrometer (Thermo Fisher Scientific, USA) at the IDeA National Resource for Quantitative Proteomics. Tryptic peptides were separated into 46 fractions on a 100 × 1.0 mm Acquity BEH C18 column (Waters) using an UltiMate 3000 UHPLC system (Thermo) with a 50 min gradient from 99:1 to 60:40 buffer A:B ratio under basic pH conditions, then consolidated into 12 super-fractions. Each super-fraction was then separated by reverse phase XSelect CSH C18 2.5 um resin (Waters) on an in-line 120 × 0.075 mm column using an UltiMate 3000 RSLCnano system (Thermo). Peptides were eluted using a 60 min gradient from 98:2 to 65:35 buffer A:B ratio. Eluted peptides were ionized by electrospray (2.4 kV) followed by mass spectrometric analysis on an Orbitrap Fusion Tribrid mass spectrometer (Thermo). MS data were acquired using the FTMS analyzer in profile mode at a resolution of 240,000 over a range of 375 to 1500 m/z. Following HCD activation, MS/MS data were acquired using the ion trap analyzer in centroid mode and normal mass range with normalized collision

energy of 28–31% depending on charge state and precursor selection range. Protein identification and quantification followed established procedures. Briefly, mass spectrometry spectra were searched using Sipros Ensemble against a protein database constructed from the metagenome. Raw search results were filtered to achieve 1% FDR (false discovery rate) at the peptide level, which was estimated using the target-decoy approach. Peptide identifications are assigned to protein or protein groups in accordance with the parsimonious rule. To avoid ambiguity in data analysis, protein groups were excluded from biological analysis. Protein quantification was achieved through Intensity-based label-free analysis using ProRata[14]. Protein abundances were quantified by the total peak height of all quantified peptides from a protein, normalized against the average total of all data sets[53–55].

Following previously described methods[56–58], the taxonomic annotations were assigned to the identified peptides based on the matched corresponding scaffold's taxonomic annotation information, which had a length greater than 1000 bp. The relative abundance of a species is expressed as the sum of the abundances of all proteins detected that belong to this species. If a protein was identified in more than one species, its abundance was equally divided among these identified species. The richness and evenness of the communities were calculated using the vegan R package, based on the total protein abundance of species[59].

### Construction of the stoichiometric model

A set of overall reactions depicting the documented metabolism of major functional populations was fit to the measured amounts of metabolites in the microcosms (Supplementary Fig. 3, Supplementary Fig. 4). The code used in fitting can be found on the Github https://github.com/thepanlab/WetlandSoil. The resulting fits provide a basis for quantifying metabolic contributions. Deviations between the inferred metabolic transformations and measured transformations indicate uncertainty in our understanding of the metabolic transformations or limitations in analytic capacity.

### Statistical analysis

Pairwise comparisons for metabolic measurement data were carried out using Student's t-test, while metabolic fluxes from modeling were analyzed using Wald type II $\chi^2$ tests. One-way or two-way ANOVA was used for comparisons among groups of more than two. Differences in protein abundance in the metaproteome were analyzed by Deseq2 R package, which is based on a model using the negative binomial distribution to account for variance and mean linkage through local regression[60–62]. The $p$-values were adjusted to $q$-values using the Benjamini and Hochberg method for multiple comparison correction[63]. Differences with $q$-value < 0.05 were regarded as statistically significant.

### Data availability

### References

1. Jansson, J. K. & Hofmockel, K. S. Soil microbiomes and climate change. *Nat. Rev. Microbiol.* **18**, 35–46 (2020).
2. Kirwan, M. L., Megonigal, J. P., Noyce, G. L. & Smith, A. J. Geomorphic and ecological constraints on the coastal carbon sink. *Nature Reviews Earth & Environment*, 1–14 (2023).
3. Candry, P., Abrahamson, B., Stahl, D. A. & Winkler, M. K. H. Microbially mediated climate feedbacks from wetland ecosystems. *Global Change Biology* (2023).
4. Bao, T., Jia, G. & Xu, X. Weakening greenhouse gas sink of pristine wetlands under warming. *Nat. Clim. Change* **13**, 462–469 (2023).
5. Chen, H., Xu, X., Fang, C., Li, B. & Nie, M. Differences in the temperature dependence of wetland $CO_2$ and $CH_4$ emissions vary with water table depth. *Nat. Clim. Change* **11**, 766–771 (2021).
6. Rillig, M. C. et al. Increasing the number of stressors reduces soil ecosystem services worldwide. *Nat. Clim. Change* 1–6 (2023).
7. Xu, X., Chen, M., Yang, G., Jiang, B. & Zhang, J. Wetland ecosystem services research: a critical review. *Glob. Ecol. Conserv.* **22**, e01027 (2020).
8. Mobilian, C. et al. Differential effects of press vs. pulse seawater intrusion on microbial communities of a tidal freshwater marsh. *Limnol. Oceanogr. Lett.* **8**, 154–161 (2023).
9. Solohin, E., Widney, S. E. & Craft, C. B. Declines in plant productivity drive loss of soil elevation in a tidal freshwater marsh exposed to saltwater intrusion. *Ecology* **101**, e03148 (2020).
10. Cavicchioli, R. et al. Scientists' warning to humanity: microorganisms and climate change. *Nat. Rev. Microbiol.* **17**, 569–586 (2019).
11. Hartmann, M. & Six, J. Soil structure and microbiome functions in agroecosystems. *Nat. Rev. Earth Environ.* **4**, 4–18 (2023).
12. Van Rossum, T., Ferretti, P., Maistrenko, O. M. & Bork, P. Diversity within species: interpreting strains in microbiomes. *Nat. Rev. Microbiol.* **18**, 491–506 (2020).
13. Lu, Z. & Imlay, J. A. When anaerobes encounter oxygen: mechanisms of oxygen toxicity, tolerance and defence. *Nat. Rev. Microbiol.* **19**, 774–785 (2021).
14. Wang, D. et al. Cross-feedings, competition, and positive and negative synergies in a four-species synthetic community for anaerobic degradation of cellulose to methane. *Mbio.* **14**, e03189–03122 (2023).
15. Berrier, D. J., Neubauer, S. C. & Franklin, R. B. Cooperative microbial interactions mediate community biogeochemical responses to saltwater intrusion in wetland soils. *FEMS Microbiol. Ecol.* **98**, fiac019 (2022).
16. Conrad, R. Soil microorganisms as controllers of atmospheric trace gases (H2, CO, CH4, OCS, N2O, and NO). *Microbiological Rev.* **60**, 609–640 (1996).
17. Stams, A. J. & Plugge, C. M. Electron transfer in syntrophic communities of anaerobic bacteria and archaea. *Nat. Rev. Microbiol.* **7**, 568–577 (2009).
18. Lee, J.-Y., Tsolis, R. M. & Bäumler, A. J. The microbiome and gut homeostasis. *Science* **377**, eabp9960 (2022).
19. Hakemian, A. S. & Rosenzweig, A. C. The biochemistry of methane oxidation. *Annu. Rev. Biochem.* **76**, 223–241 (2007).
20. He, S. et al. Patterns in wetland microbial community composition and functional gene repertoire associated with methane emissions. *mBio* **6**, 10.1128/mbio.00066-00015, https://doi.org/10.1128/mbio.00066-15 (2015).
21. Martins, P. D., Frank, J., Mitchell, H., Markillie, L. M. & Wilkins, M. J. Wetland sediments host diverse microbial taxa capable of cycling alcohols. *Appl. Environ. Microbiol.* **85**, e00189–00119 (2019).
22. Noyce, G. L., Smith, A. J., Kirwan, M. L., Rich, R. L. & Megonigal, J. P. Oxygen priming induced by elevated CO2 reduces carbon accumulation and methane emissions in coastal wetlands. *Nat. Geosci.* **16**, 63–68 (2023).
23. Chen, X. et al. Priming effects of root exudates on the source-sink stability of benzo [a] pyrene in wetlands: a microcosm experiment. *J. Hazard. Mater.* **429**, 128364 (2022).
24. Wilmoth, J. L. et al. The role of oxygen in stimulating methane production in wetlands. *Glob. Change Biol.* **27**, 5831–5847 (2021).
25. Bittleston, L. S., Gralka, M., Leventhal, G. E., Mizrahi, I. & Cordero, O. X. Context-dependent dynamics lead to the assembly of functionally distinct microbial communities. *Nat. Commun.* **11**, 1440 (2020).

26. Gralka, M., Szabo, R., Stocker, R. & Cordero, O. X. Trophic interactions and the drivers of microbial community assembly. *Curr. Biol.* **30**, R1176–R1188 (2020).

27. Canfield, D. E. & Farquhar, J. Animal evolution, bioturbation, and the sulfate concentration of the oceans. *Proc. Natl Acad. Sci. USA* **106**, 8123–8127 (2009).

28. Santos, A. M. D. et al. Lactate as an effective electron donor in the sulfate reduction: impacts on the microbial diversity. *Environ. Technol.* **43**, 3149–3160 (2022).

29. Ward, N. D. et al. Representing the function and sensitivity of coastal interfaces in Earth system models. *Nat. Commun.* **11**, 2458 (2020).

30. Segarra, K. et al. High rates of anaerobic methane oxidation in freshwater wetlands reduce potential atmospheric methane emissions. *Nat. Commun.* **6**, 7477 (2015).

31. Timmers, P. H. et al. Anaerobic oxidation of methane associated with sulfate reduction in a natural freshwater gas source. *ISME J.* **10**, 1400–1412 (2016).

32. Lawson, C. E. et al. Common principles and best practices for engineering microbiomes. *Nat. Rev. Microbiol.* **17**, 725–741 (2019).

33. Des Marais, D. L., Hernandez, K. M. & Juenger, T. E. Genotype-by-environment interaction and plasticity: exploring genomic responses of plants to the abiotic environment. *Annu. Rev. Ecol., Evolution, Syst.* **44**, 5–29 (2013).

34. Chebbi, A., Sinopoli, A., Abotaleb, A. & Bicer, Y. Photocatalytic conversion of carbon dioxide, methane, and air for green fuels synthesis. *Catalysis Science & Technology* (2023).

35. Lovley, D. R., Dwyer, D. F. & Klug, M. J. Kinetic analysis of competition between sulfate reducers and methanogens for hydrogen in sediments. *Appl. Environ. Microbiol.* **43**, 1373–1379 (1982).

36. Dar, S. A., Kleerebezem, R., Stams, A. J., Kuenen, J. G. & Muyzer, G. Competition and coexistence of sulfate-reducing bacteria, acetogens and methanogens in a lab-scale anaerobic bioreactor as affected by changing substrate to sulfate ratio. *Appl. Microbiol. Biotechnol.* **78**, 1045–1055 (2008).

37. Ye, R. et al. pH controls over anaerobic carbon mineralization, the efficiency of methane production, and methanogenic pathways in peatlands across an ombrotrophic–minerotrophic gradient. *Soil Biol. Biochem.* **54**, 36–47 (2012).

38. Nguyen, D. & Khanal, S. K. A little breath of fresh air into an anaerobic system: How microaeration facilitates anaerobic digestion process. *Biotechnol. Adv.* **36**, 1971–1983 (2018).

39. Lim, J. W. & Wang, J.-Y. Enhanced hydrolysis and methane yield by applying microaeration pretreatment to the anaerobic co-digestion of brown water and food waste. *Waste Manag.* **33**, 813–819 (2013).

40. Banerjee, S. & van der Heijden, M. G. Soil microbiomes and one health. *Nat. Rev. Microbiol.* **21**, 6–20 (2023).

41. Rillig, M. C. et al. The role of multiple global change factors in driving soil functions and microbial biodiversity. *Science* **366**, 886–890 (2019).

42. Yang, G. et al. Multiple anthropogenic pressures eliminate the effects of soil microbial diversity on ecosystem functions in experimental microcosms. *Nat. Commun.* **13**, 4260 (2022).

43. Loreau, M. et al. Biodiversity and ecosystem functioning: current knowledge and future challenges. *Science* **294**, 804–808 (2001).

44. Li, Y. et al. Combined inactivation of the Clostridium cellulolyticum lactate and malate dehydrogenase genes substantially increases ethanol yield from cellulose and switchgrass fermentations. *Biotechnol. Biofuels* **5**, 1–13 (2012).

45. Diamond, S. et al. Mediterranean grassland soil C–N compound turnover is dependent on rainfall and depth, and is mediated by genomically divergent microorganisms. *Nat. Microbiol.* **4**, 1356–1367 (2019).

46. Bushnell, B. BBTools software packag. *e* (2014).

47. Nurk, S., Meleshko, D., Korobeynikov, A. & Pevzner, P. A. metaSPAdes: a new versatile metagenomic assembler. *Genome Res.* **27**, 824–834 (2017).

48. Hyatt, D. et al. Prodigal: prokaryotic gene recognition and translation initiation site identification. *BMC Bioinforma.* **11**, 1–11 (2010).

49. Aramaki, T. et al. KofamKOALA: KEGG Ortholog assignment based on profile HMM and adaptive score threshold. *Bioinformatics* **36**, 2251–2252 (2020).

50. Menzel, P., Ng, K. L. & Krogh, A. Fast and sensitive taxonomic classification for metagenomics with Kaiju. *Nat. Commun.* **7**, 11257 (2016).

51. Kang, D. D. et al. MetaBAT 2: an adaptive binning algorithm for robust and efficient genome reconstruction from metagenome assemblies. *PeerJ* **7**, e7359 (2019).

52. Chaumeil, P.-A., Mussig, A. J., Hugenholtz, P. & Parks, D. H. (Oxford University Press, 2020).

53. Griffin, N. M. et al. Label-free, normalized quantification of complex mass spectrometry data for proteomic analysis. *Nat. Biotechnol.* **28**, 83–89 (2010).

54. Vogel, C. & Marcotte, E. M. Calculating absolute and relative protein abundance from mass spectrometry-based protein expression data. *Nat. Protoc.* **3**, 1444–1451 (2008).

55. Matzke, M. M. et al. A comparative analysis of computational approaches to relative protein quantification using peptide peak intensities in label-free LC-MS proteomics experiments. *Proteomics* **13**, 493–503 (2013).

56. Cheng, K. et al. MetaLab: an automated pipeline for metaproteomic data analysis. *Microbiome* **5**, 1–10 (2017).

57. Xiao, J. et al. Metagenomic taxonomy-guided database-searching strategy for improving metaproteomic analysis. *J. Proteome Res.* **17**, 1596–1605 (2018).

58. Easterly, C. W. et al. metaQuantome: an integrated, quantitative metaproteomics approach reveals connections between taxonomy and protein function in complex microbiomes. *Mol. Cell. Proteom.* **18**, S82–S91 (2019).

59. Dixon, P. VEGAN, a package of R functions for community ecology. *J. Vegetation Sci.* **14**, 927–930 (2003).

60. Fremin, B. J., Sberro, H. & Bhatt, A. S. MetaRibo-Seq measures translation in microbiomes. *Nat. Commun.* **11**, 3268 (2020).

61. Lin, Y., Wang, L., Xu, K., Li, K. & Ren, H. Revealing taxon-specific heavy metal-resistance mechanisms in denitrifying phosphorus removal sludge using genome-centric metaproteomics. *Microbiome* **9**, 1–17 (2021).

62. Debeljak, P., Bayer, B., Sun, Y., Herndl, G. J. & Obernosterer, I. Seasonal patterns in microbial carbon and iron transporter expression in the Southern Ocean. *Microbiome* **11**, 187 (2023).

63. Love, M., Anders, S. & Huber, W. Differential analysis of count data–the DESeq2 package. *Genome Biol.* **15**, 10–1186 (2014).

## Acknowledgements

## Author contributions

D.W. and C.P. designed the study. P.C., F.Z., and M.H.W. sampled wetland soil. D.W., N.Q.W., and M.J.M. performed the incubation of wetland soil. D.W., R.S.T., and J.Z. conducted the metabolite analysis. D.W. performed metagenomics and metaproteomics analysis. D.W., K.A.H., Y.L., Z.S., and D.A.S. performed the modeling. D.W., P.C., F.Z., K.B.D., and D.A.S. performed biological interpretation. C.P. and M.H.W. served as the principal investigator of the funding sources. D.W. and C.P. drafted the manuscript. All authors contributed to the revision and approved the final manuscript.

## Competing interests

The authors declare no competing interests.

## Additional information

**Supplementary information** The online version contains supplementary material available at
https://doi.org/10.1038/s41522-024-00525-5.

**Correspondence** and requests for materials should be addressed to Chongle Pan.

**Reprints and permissions information** is available at
http://www.nature.com/reprints

**Publisher's note** Springer Nature remains neutral with regard to jurisdictional claims in published maps and institutional affiliations.